Magnetic Ordering in $Dy(OH)_3$ and $Ho(OH)_3$ †

C. A. Catanese* and H. E. Meissner‡
Yale University, Becton Center, New Haven, Connecticut 06520
(Received 22 March 1973)

Measurements are reported on the low-temperature (1–16 K) magnetic susceptibilities and specific heats of the hexagonal compounds $Dy(OH)_3$ and $Ho(OH)_3$. $Dy(OH)_3$ is shown to be highly anisotropic below 4 K, with the magnetic moment strongly constrained to lie along the c axis. At 3.48 K, the spin system undergoes a phase transition to a ferromagnetic ordered state; this transition is dominated by the long-range magnetic dipole-dipole interactions. The effective Hamiltonian of the spin system is shown to be accurately represented by an Ising Hamiltonian, a scalar form which is particularly tractable to theoretical analysis. Above 4 K, the susceptibility and the specific-heat behavior are strongly influenced by the presence of low-lying energy levels and it is shown that the specific-heat behavior predicted on the basis of spectroscopically observed states agrees accurately with the experimental results. $Ho(OH)_3$ is very similar to $Dy(OH)_3$. Below 4 K the spins align parallel to the c axis. At 2.54 K, $Ho(OH)_3$ undergoes a transition to a ferromagnetic ordered state under the dominance of magnetic dipole-dipole interactions. Above 4 K the susceptibility and specific heat are strongly influenced by the presence of low-lying excited states, and again this behavior is accurately accounted for on the basis of the spectroscopically observed states.

I. INTRODUCTION

In an earlier report on the magnetic properties of the rare-earth hydroxides[1] it was pointed out that several of the compounds in this series—notably Gd, Tb, Dy and Ho (hydroxide)–exhibit magnetic effects which might make them of importance to the basic understanding of ordering phenomena in insulators. In a recent paper[2] $Tb(OH)_3$ was shown to be an example of a nearly ideal Ising system with a ferromagnetic transition at 3.7 K, and an accurate solution for the near-neighbor interactions was deduced. Similarly, an accurate solution has been obtained for $Gd(OH)_3$,[3] which was shown to order antiferromagnetically at 0.9 K under the influence of a dominant nearest-neighbor exchange interaction.

It is clearly of interest to make a similar study of the remaining two strongly magnetic compounds in the series: $Dy(OH)_3$ and $Ho(OH)_3$. In this paper we present the results of specific-heat, magnetic-moment, and susceptibility measurements on these two compounds. Our measurements at liquid-helium temperatures (1 – 4 K) show $Dy(OH)_3$ and $Ho(OH)_3$ to be strongly anisotropic, Ising-like magnetic systems with phase transitions in this temperature region. In these respects the two compounds are strikingly similar to one another and to $Tb(OH)_3$. At higher temperatures the behavior in $Dy(OH)_3$ and $Ho(OH)_3$ is strongly modified by the presence of low-lying excited states.

There is excellent agreement between the specific heat and susceptibility measurements as to the ordering temperatures—3.48 K in $Dy(OH)_3$ and 2.54 K in $Ho(OH)_3$—and strong indications from the susceptibility measurements that the transition is ferromagnetic in both cases. Analysis of the low-temperature specific heat in $Dy(OH)_3$, and the magnetic internal energy of $Ho(OH)_3$, yielded values for the Weiss Θ of 4.4 and 4.2 K, respectively. Comparison of these values with the theoretical dipolar contributions to Θ leads to the conclusion that the net nondipolar interactions are antiferromagnetic in character and that the dipolar interactions therefore play a very important, if not dominant, role in the ferromagnetic ordering.

Estimates of the wave functions and energy level schemes in these two compounds are available from the spectroscopic work reported by Scott[4] on $Dy(OH)_3$ and $Y(OH)_3$: Ho. Comparison of the experimental values for the saturation magnetization and anisotropy with the values calculated from these spectroscopic results yielded excellent agreement. Analysis of the Schottky specific heat above 4 K in terms of these spectroscopic energy levels shows that the observed behavior is accurately accounted for.

There is thus presented a fairly complete description of the low-temperature bulk property effects in $Dy(OH)_3$ and $Ho(OH)_3$ and an accurate correlation of this description with the spectroscopic energy level scheme.

II. EXPERIMENTAL METHODS

The experiments done in the course of this work consisted primarily in measurements of three quantities: magnetic moments, magnetic susceptibility, and specific heat. The methods used in these measurements are described briefly in this section. The apparatuses used were the same ones used in the references given below and the reader is referred to those references for complete details. There is also to be found in Refs. 3 and 5 extensive

TABLE I. Summary of physical properties (Refs. 5 and 12).

		$Dy(OH)_3$		$Ho(OH)_3$
Crystal group		C_{3h}		C_{3h}
Lattice constants				
c		3.56 Å		3.53 Å
a		6.26 Å		6.24 Å
Density		5.86 g/cm^3		6.02 g/cm^3
R^{3+} ground term		$9f$, $^6H_{15/2}$		$10f$, $^5I_8$
R^{3+} nuclear isotopes	Dy^{161}	Dy^{163}	Dy^{162}	Ho^{165}
Isotopic spin	$\frac{5}{2}$	$\frac{5}{2}$	0	$\frac{7}{2}$
Isotope abundance	19%	25%	56%	100%
Hyperfine constant $A/g_{\parallel}$	3.93×10^{-3}	5.46×10^{-3}		3.05×10^{-2}

data on crystal structure, density, lattice parameters, etc. of the hydroxide series. For convenience, some of this data is summarized in Table I.

A. Magnetization

Measurements of the magnetization M in fields up to 14 kOe from 1–4 K were made using a Foner-type magnetometer, details of which have been given elsewhere.[6] The samples were small (~ 1 mg), needle-shaped single crystals. The high sensitivity (~ 2×10^{-4} emu) of the apparatus enabled us to measure even these small samples to a relative accuracy of 0.1%. Taking into consideration the calibration procedure and the mass of the sample, the absolute accuracy of the magnetization results was about 1%. Particular care was taken to ensure that the field was closely aligned with the appropriate crystal axis. For measurements parallel to the c axis, where the moment is high, the alignment was accurate to about 3°. Perpendicular to the c axis the moment is far smaller and the field alignment, closer than 0.2°, virtually eliminated errors due to anisotropy.

B. Susceptibility

The zero-field susceptibility χ at liquid-hydrogen temperatures was measured using the technique of McKim and Wolf[7] which relates χ to the change in mutual inductance when a sample is removed from a concentric coil pair. The samples were bundles of aligned single crystals with weights of the order of 10 mg. The relative accuracy for these measurements was estimated at about 0.1% and the absolute accuracy about 0.5%.

Frequency-dependent domain-relaxation effects precluded the use of the mutual-inductance technique near the ordering temperatures. For this temperature region—below 4.2 K—χ was calculated from the low-field moments as measured with an inductance-coil–ballistic-galvanometer setup.[2] In these measurements the sample was snatched quickly out of a coil and the moment determined from the integrated induced current on a ballistic galvanometer in series with the coil. This method was accurate to 4% at the lowest moments recorded—and very well suited for this low-field work. Again, the samples were accurately aligned needle-shaped single crystals.

C. Specific Heat

Measurements of the specific heat C were carried out with a heat-pulse calorimeter method, using a cryostat equipped for both He^3 and He^4 cooling.[5] The samples were large amounts (40–60 g) of polycrystalline powder mixed with a small amount of grease to promote thermal contact. The contributions of the calorimeter and the grease to the measured heat capacity were determined in a separate measurement and subtracted. The uncertainty in this contribution is the main source of error. This error was estimated to be negligible below 5 K and rising to about 2% at 10 K.

The small temperature differentials needed to accurately determine specific heat were measured using calibrated germanium and carbon resistance thermometers. For all of the magnetic measurements, the temperatures were found from the vapor pressure above the coolant after correction for hydrostatic head pressure.

III. $Dy(OH)_3$: DATA AND ANALYSIS

In an axially symmetric crystalline field the $4f^9$, $6H_{15/2}$ ground term of the free Dy^{3+} ion is split into eight Kramers doublets, each state being an eigenfunction of J_z where z is along the symmetry axis. If the symmetry is lowered further to the C_{3h} group of the rare earth hydroxides, it can be shown very generally that there will be admixing allowed only between states which differ by 6 in J_z.

The crystal field effects in $Dy(OH)_3$ were the subject of an absorption spectroscopy study reported by Scott.[4] Scott found that at 4.2 K the ground state was a nearly pure doublet with $J_z = \pm\frac{15}{2}$ and that the first excited state was a doublet with an energy of 15.6 cm^{-1}. However the number of absorption lines was too sparse at 4.2 K to permit a full determina-

TABLE II. Summary of spectroscopic data (Ref. 4).

	$Dy(OH)_3$		$Y(OH)_3$: Ho
	77 K	4.2 K	77 K
Crystal field parameters	$B_2^0 = 209.4 \pm 6.5$ cm^{-1}		$B_2^0 = 246.0 \pm 3.4$ cm^{-1}
	$B_4^0 = -75.5 \pm 3.5$ cm^{-1}		$B_4^0 = -56.7 \pm 1.2$ cm^{-1}
	$B_6^0 = -40.1 \pm 1.9$ cm^{-1}		$B_6^0 = -39.8 \pm 0.3$ cm^{-1}
	$B_6^6 = 541.8 \pm 26.5$ cm^{-1}		$B_6^6 = 543.6 \pm 3.3$ cm^{-1}
Ground state	$0.91\,\vert \pm\frac{15}{2}\rangle - 0.15\,\vert \pm\frac{3}{2}\rangle + 0.39\,\vert \mp\frac{9}{2}\rangle$	$0.99\,\vert \pm\frac{15}{2}\rangle - 0.10\,\vert \pm\frac{3}{2}\rangle + 0.13\,\vert \mp\frac{9}{2}\rangle$	$0.93\,\vert \pm 7\rangle + 0.31\,\vert \pm 1\rangle + 0.15\,\vert \mp 5\rangle$
Low-lying excited states	$-0.41\,\vert \pm\frac{15}{2}\rangle - 0.19\,\vert \pm\frac{3}{2}\,\vert + 0.89\,\vert \mp\frac{9}{2}\rangle$ at 7.80 cm^{-1}	first excited state at 15.6 cm^{-1}	$0.59\,\vert +6\rangle + 0.55\,\vert 0\rangle + 0.59\,\vert -6\rangle$ at 11.1 cm^{-1}
	$+0.13\,\vert \pm\frac{13}{2}\rangle - 0.17\,\vert \pm\frac{1}{2}\rangle + 0.98\,\vert \mp\frac{11}{2}\rangle$ at 21.5 cm^{-1}		$0.71\,\vert +6\rangle + 0.71\,\vert -6\rangle$ at 75 cm^{-1}
	$+0.88\,\vert \pm\frac{7}{2}\rangle - 0.47\,\vert \mp\frac{5}{2}\rangle$ at 27 cm^{-1}		
	$+0.98\,\vert \pm\frac{13}{2}\rangle - 0.10\,\vert \pm\frac{1}{2}\rangle - 0.15\,\vert \mp\frac{11}{2}\rangle$ at 54.7 cm^{-1}		

tion of crystal field parameters or even to determine the energies of the other low-lying levels. In similar measurements at 77 K, it was found that the ground state had become a somewhat less pure $J_z = \pm\frac{15}{2}$ doublet and the first excited state had lowered to an energy of 7.8 cm^{-1}. With higher lying states populated at 77 K, Scott was able to complete a full crystal field determination which revealed further low-lying states with energies of 21.5, 27, and 54.7 cm^{-1}. A summary of Scott's crystal field results is included in Table II. This data will be used extensively to correlate with and explain the bulk property results described below.

A. Experimental Results

1. Magnetic Measurements

The high-field magnetization of $Dy(OH)_3$ at liquid-helium temperatures was measured on a needle-shaped single crystal sample weighing 0.8 mg and having an aspect ratio of 20:1. The magnetization with the applied field parallel ($M_\parallel$) and perpendicular ($M_\perp$) to the c axis is shown in Fig. 1. $M_\parallel$ saturates quickly with increasing field, and from the data at 1.1 K we extract a value of

$$M_{sat} = 1405 \pm 15 \text{ emu/cm}^3$$

for the saturation magnetization, and an upper limit of

$$\chi_\parallel < 1.5 \times 10^{-3} \text{ emu/cm}^3$$

for the high-field slope. The magnitude of this saturation moment is quite large, comparable to that of iron ($M_{sat} \approx 1700$ emu/cm^3) and nickel ($M_{sat} \approx 500$ emu/cm^3). No hysteresis was found in the $M_\parallel$-H curves except at the lowest temperature measured, 1.1 K, at which point the coercive field is only 3 Oe.

The high anisotropy in the magnetic system is evident from Fig. 1 $M_\perp$ is orders of magnitudes smaller than $M_\parallel$—note the enhanced scale for $M_\perp$ at the right—and does not saturate in these fields. The susceptibility estimated from Fig. 1 is

$$\chi_\perp = 5 \times 10^{-4} \text{ emu/cm}^3.$$

From the enormous difference between $M_\parallel$ and $M_\perp$, it is evident that the moments in $Dy(OH)_3$ are very strongly constrained to lie along the c axis, marking

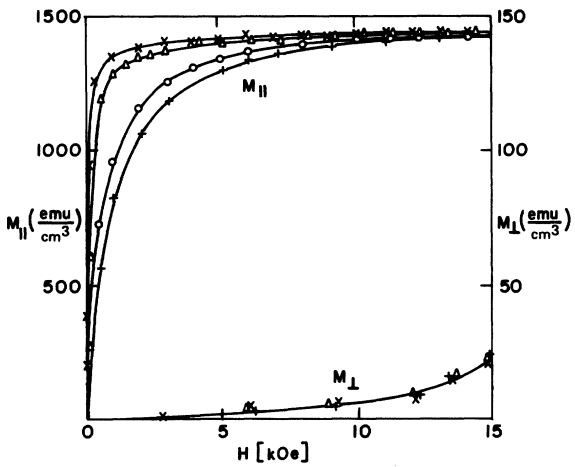

FIG. 1. High field moment of $Dy(OH)_3$ for a series of temperatures in the liquid-helium range: 4.2 K (+), 3.8 K (○), 2.4 K (△), 1.1 K (×). The values of $M_\perp$ (lower curves) are read from the expanded scale at the right, making the actual anisotropy even greater than first appears in the figure.

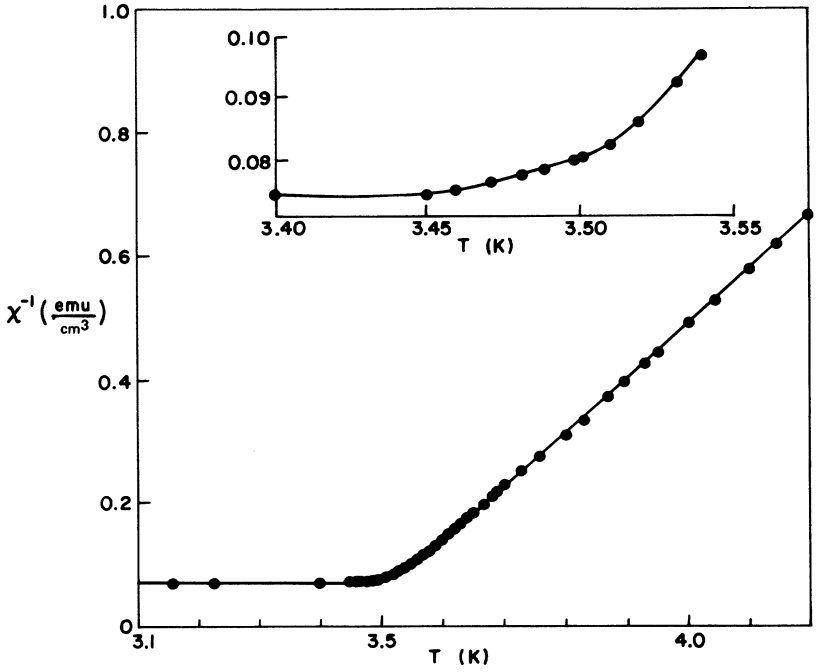

FIG. 2. Susceptibility of $Dy(OH)_3$ in the neighborhood of $T_C = 3.48$ K. It can be seen from the enlarged insert that there is no clear breaking indicating T_C and that χ is still varying below 3.48 K.

this as one of the most anisotropic systems known.

The low-field magnetization of a single crystal of $Dy(OH)_3$, measured by the ballistic-galvanometer technique, was vanishingly small for fields perpendicular to the c axis in agreement with the magnetometer results given above. With the field along the c axis the response was quite large and allowed an accurate determination of $M_{\parallel}$ in fields as small as 10 Oe. The zero-field susceptibility was derived from these measurements by means of a prescription given by Belov and Goryaga[8] and also Kouvel and Fisher.[9] If the quantity H/M is expanded in powers of M, assuming a Brillouin functional dependence, then as M goes to zero H/M, the inverse susceptibility, varies as M^2. χ^{-1} is found by extrapolating the graph of H/M vs M^2 to $M^2 = 0$, and the result of this process for $Dy(OH)_3$ is shown in Fig. 2. χ^{-1} decreases rapidly as the temperature decreases, until about 3.5 K, below which χ^{-1} assumes a roughly constant value. This behavior is characteristic of a ferromagnet near its phase transition: χ^{-1} decreases with decreasing temperature down to T_C, the Curie temperature, below which it is constant and equal to the demagnetizing factor. The enlarged inset in Fig. 2 shows that χ^{-1} attains a constant value very gradually, with no detectable break defining a Curie temperature.

To extract a value of T_C, it is assumed[9] that as T approaches T_C from above, the susceptibility varies as

$$\chi^{-1} \propto (T - T_C)^{\gamma}. \tag{1}$$

If one defines the quantity

$$T^*(T) = \frac{\chi^{-1}}{d\chi^{-1}/dT}\ , \tag{2}$$

then, as T approaches T_C, $T^*(T)$ should approach the linear function $(T - T_C)/\gamma$. The Curie point is identified as T for which $T^* = 0$. Figure 3 shows the graph of T^* obtained by numerical differentiation of the χ data, from which the Curie temperature was found to be

$$T_C = 3.48 \pm 0.02 \text{ K}$$

by a short extrapolation. This result agrees precisely with the value found from the specific-heat data described later in this section.

The curves of H/M vs M^2 contain a well-defined, abrupt break in the slope for $T \ll 3.5$ K. This "kink" is generally identified with the spontaneous magnetization M_{sp}, and the plot of M_{sp} vs T is given in Fig. 4. A surprising feature of this curve is the low value of ~930 emu/cm^3 which M_{sp} approaches at low temperatures, compared to the saturation moment of 1405 emu/cm^3.

This low value of M_{sp}, corresponding to 15% of the spins reversed from the ferromagnetic state at $T = 0$, may be a result of the nonellipsoidal shape of the single crystals: The rough ends of the crystals very likely give rise to high local demagnetizing fields, locking some small domains near the end in a state of magnetization reversed from the bulk.

Such end effects may also be responsible for the fact that χ^{-1} does not attain a constant value down to 3.3 K (Fig. 2), in spite of the fact that

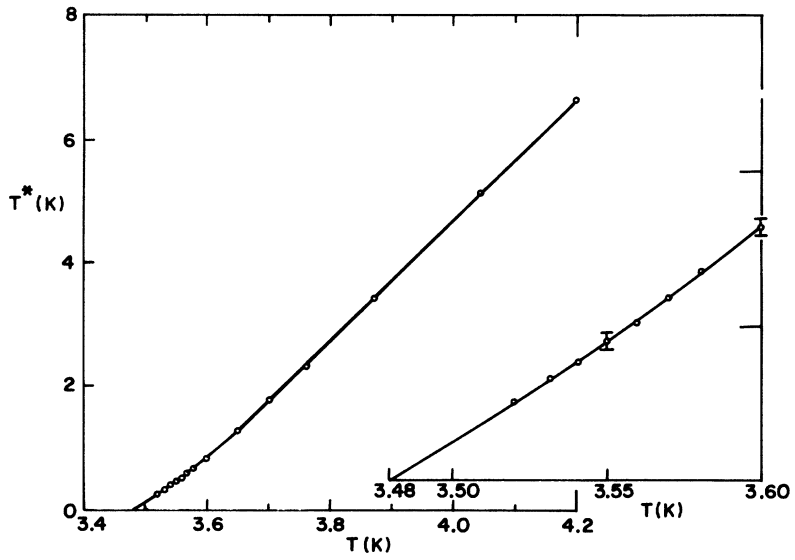

FIG. 3. $T^* - T$ near the ordering temperature in $Dy(OH)_3$. From the enlarged insert it can be seen that there is very little error resulting from the extrapolation to $T_C = 3.48$ K.

both the T^* analysis and the specific heat behavior unambiguously identify T_C as 3.48 K. This "smearing out" of the ordering behavior could well be due to the variation in the local environment of the spins near the ends of the sample. It is, in fact, for this reason that we have not pursued the analysis of χ to determine the γ of Eq. (1): Any conclusion about the details of critical phenomena which is deduced from experiments on nonellipsoidal samples is, at this point, quite unjustifiable.

The susceptibility of a single-crystal needle parallel to the c axis was measured in the liquid-hydrogen-temperature range (14–20 K) using the ac inductance technique. The $\chi^{-1}-T$ curve (Fig. 5) appears to be a reasonably straight line, suggestive of Curie–Weiss-law behavior:

$$\chi^{-1} = (T - \Theta)/\lambda \ . \tag{3}$$

But the low-temperature Curie constant of $Dy(OH)_3$ is $\lambda = 0.158$ emu/g (Sec. III B 1) and the slope of the curve clearly deviates from this value of $1/\lambda$, shown as the dotted line in the figure. This is not unexpected, since the low-lying excited states become populated at these temperatures and the exact analytical expression for χ will be a complicated function of excited-state levels, eigenfunctions, and interaction constants.

2. *Specific Heat*

The specific heat of $Dy(OH)_3$ between 0.6 and 16 K is plotted in Fig. 6 as the dimensionless quantity C/R, where R is the gas constant. The prominent spike at about 3.5 K is the familiar λ anomaly of the ferromagnetic phase transition noted in the susceptibility results. This peak is very well defined and allows accurate determination of T_C as

$$T_C = 3.48 \pm 0.01 \text{ K} \ .$$

This value agrees exactly with T_C as obtained from χ measurements. Above T_C the specific heat rises to a broad maximum at 12 K; in this range the magnetic contribution to C/R should be a decreasing function of temperature, and the behavior dominated by lattice and Schottky contributions. Below the λ anomaly C/R decreases monotonically and, down to the lowest temperature measured, there is little indication of a significant hyperfine contribution. These individual contributions to C/R will be considered further in Sec. III B 2.

B. Analysis

1. *Magnetic Measurements*

Below 4.2 K the first excited state at 15.6 cm^{-1} is virtually unoccupied and the ground doublet can be regarded as totally isolated. In a large applied field the saturation magnetization of such a doublet is

$$M_{sat} = N g_J \mu_B \langle s_z \,|\, J_z \,|\, s_z \rangle \ , \tag{4}$$

where N ($= 1.60 \times 10^{22}$) is the number of spins per cm^3, g_J ($= \frac{4}{5}$) is the Dy^{3+} ground term Landé factor, μ_B is the Bohr magneton and $\langle s_z \,|\, J_z \,|\, s_z \rangle$ is the expectation value of J_z in the ground doublet. Scott's[4] ground-state wave function is

$$0.99 \,|\, \pm\tfrac{15}{2} \rangle - 0.10 \,|\, \pm\tfrac{3}{2} \rangle + 0.13 \,|\, \mp\tfrac{9}{2} \rangle$$

and the value of M_{sat} calculated from Eq. (4) is $M_{sat} = 1412$ emu/cm^3, in good agreement with the experimental value of 1405 ± 15 emu/cm^3. From this result we also calculate the Curie constant

$$\lambda = M_{sat}^2 / Nk \tag{5}$$

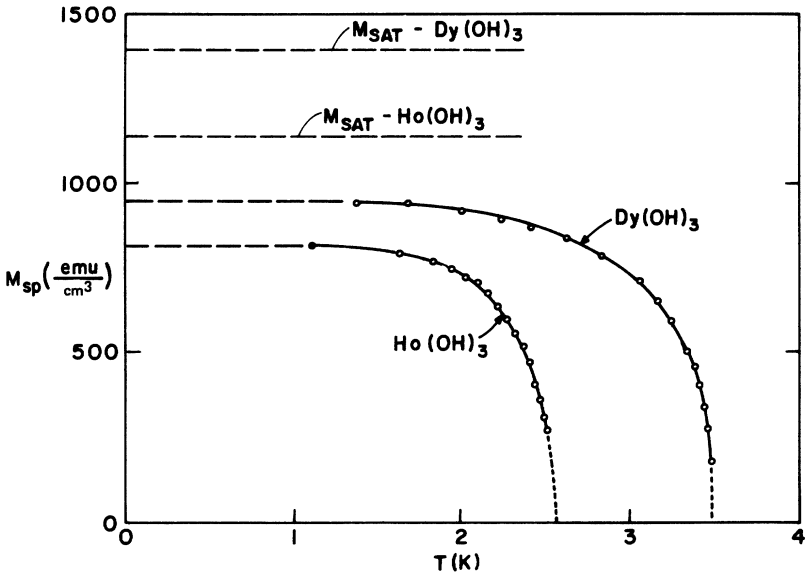

FIG. 4. Spontaneous magnetization of $Dy(OH)_3$ and $Ho(OH)_3$ along c axis. The $T=0$ intercept will clearly fall far below the measured saturation magnetization M_{sat}. This discrepancy is probably due to reversed domains near the ends of the sample.

to be 0.92 emu/cm^3 or 0.158 emu/g.

The theoretical value expected for $M_\perp$ is identically zero, due to the vanishing of the matrix elements of J_x within the ground doublet. The small value of $M_\perp$ found experimentally is probably due to the admixing of excited states into the ground doublet via the Zeeman Hamiltonian—the familiar Van Vleck susceptibility. Without a knowledge of the excited-state wave functions at 4.2 K, it is not possible to check this quantitatively.

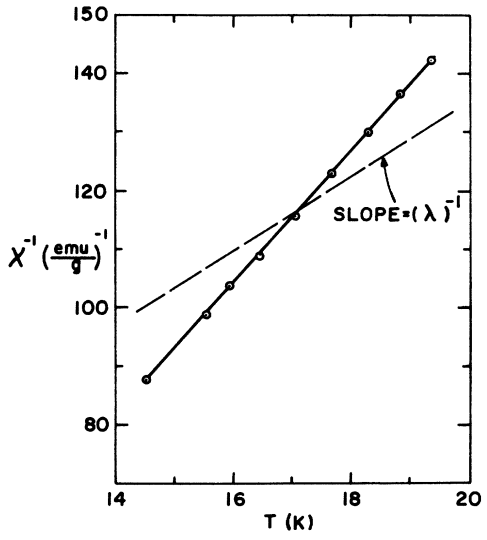

FIG. 5. $\chi^{-1}-T$ for $Dy(OH)_3$ along the c axis in the liquid-hydrogen temperature range. The dashed curve has a slope equal to $1/\lambda=6.4$, the inverse low-temperature Curie constant. The deviation of the experimental values from this slope is due primarily to the low-lying excited states.

2. Specific Heat

The four major sources contributing to the total specific heat of $Dy(OH)_3$ between 0.6 and 16 K will be considered in detail in this section.

a. Hyperfine specific heat. The decrease in C/R with decreasing temperature near 0.6 K is evidence that the main hyperfine contribution C_{hf} is at still lower temperatures. The analytical treatment of C_{hf} for these "high temperatures" is analogous to the familiar high temperature series expansion method for magnetic ions. In systems with a doubly degenerate ground state and an axially symmetric crystalline field, the lowest multipole hyperfine interaction term is[10]

$$\mathcal{H}_{hf}=AS_zI_z+B(S_xI_x+S_yI_y) \tag{6}$$

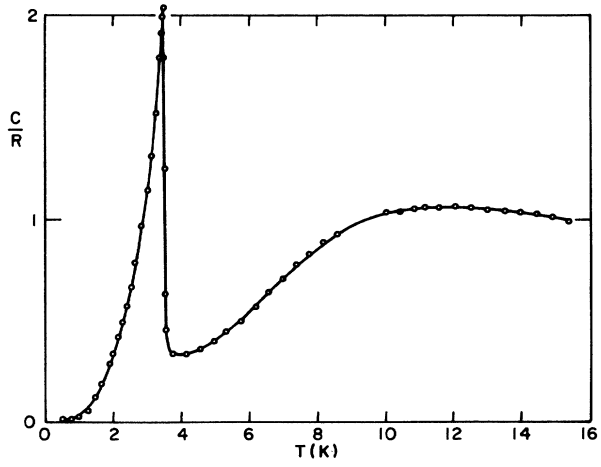

FIG. 6. Specific heat of $Dy(OH)_3$. The prominent peak sharply defines the Curie temperature at 3.48 ± 0.01 K.

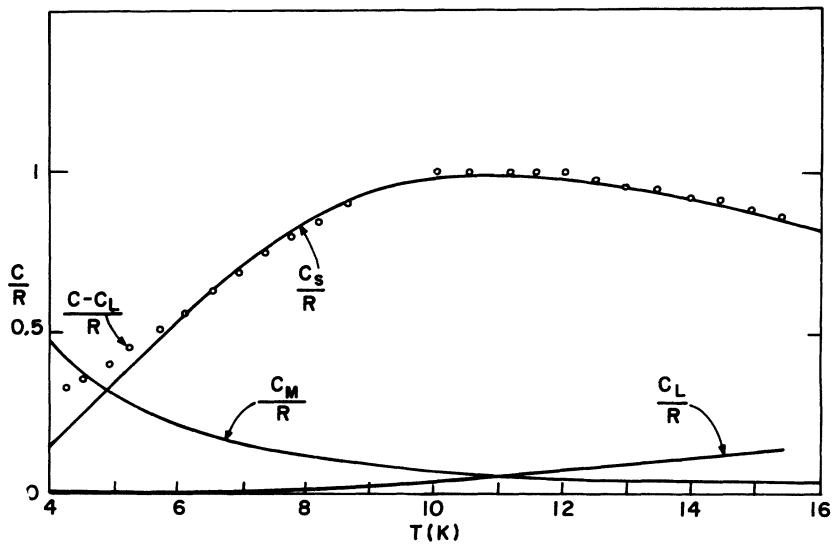

FIG. 7. Contributions to the specific heat of $Dy(OH)_3$. C_L is the lattice specific heat, taken to be equal to the total specific heat of $La(OH)_3$. C_M is an estimate to the magnetic specific heat given by the lowest order dipolar contribution. C_S is the Schottky estimate and $C - C_L$ (the data points) are the experimental results less the lattice estimates.

and the lowest-order specific-heat term is

$$C_{hf}/R = (1/T^2)\tfrac{1}{9}S(S+1)I(I+1)(A^2+2B^2). \quad (7)$$

Here I is the nuclear spin and $S = \frac{1}{2}$. The constants A and B may be found from the relation[11]

$$A/g_{\parallel} = B/g_{\perp} = \text{const}, \quad (8)$$

which relation is independent of the particular crystalline field within a given ground term. The constants for Dy^{3+} isotopes have been found from measurements on dysprosium ethylsulfate, [12] and averaging over the isotopes using the natural abundances (Table I) we find

$$C_{hf}/R = 0.002/T^2$$

for the hyperfine specific heat. This term is very small—less than the error limits on C—over the entire range of temperatures investigated.

b. Lattice specific heat. An estimate of the lattice specific heat of all the rare-earth hydroxides is obtained from a measurement of the total specific heat of $La(OH)_3$. $La(OH)_3$ is a diamagnetic compound, isostructural with the rest of the rare-earth hydroxides and has no low-lying excited states. Measurements of C_L for several rare-earth hydroxide compounds[13] in which the lattice specific heat is easily isolated showed that C_L agreed to about 10% with the total C of $La(OH)_3$. The total specific heat of $La(OH)_3$, which is shown in Fig. 7, will therefore be used as the estimate of C_L in $Dy(OH)_3$.

c. Magnetic specific heat. The magnetic specific heat above T_C may be expressed[14] as a power series in $1/T$:

$$\frac{C_M}{R} = \sum_{n=2}^{\infty} \frac{C_n}{T^n}. \quad (9)$$

This series has a radius of convergence of $1/T = 1/T_C$ and the singularity at T_C corresponds to the ferromagnetic anomaly. The coefficients C_n are functions of the interaction constants and in simple systems very accurate experimental results can often be coupled with theoretical expressions for C_n to provide solutions for the interaction constants. In $Dy(OH)_3$, the uncertainties in the lattice specific heat and the excited state population make it impossible to separate out C_n with the required accuracy to permit a determination of interaction constants.

At temperatures well above T_C, only the first term, C_2/T^2, contributes significantly to the sum in Eq. (7). An estimate of the magnitude of C_2 in $Dy(OH)_3$ can be obtained from the theoretical value calculated assuming only dipolar interactions operative and only the ground doublet occupied:

$$C_2^{dip} = \frac{\mu_B^4}{32k^2}\left(g_{\parallel}^4 \sum_j \frac{1}{r_{ij}^6} - 6g_{\parallel}^4 \sum_j \frac{z_{ij}^2}{r_{ij}^8} + 9g_{\parallel}^4 \sum_j \frac{z_{ij}^4}{r_{ij}^{10}}\right), \quad (10)$$

where k is the Boltzmann constant, r and z are spatial distances between sites, and the sums are over all neighbors of a reference site. A computer sum yielded the value $C_2^{dip} = 7.7\ \text{K}^2$ in $Dy(OH)_3$. Since the dipolar interaction will be shown to be dominant in $Dy(OH)_3$ (Sec. III C), it can be assumed that the true value of C_2 will not be significantly larger than C_2^{dip}; but fortuitous cancellations with nondipolar terms can result in a value of D_2 which is much smaller than C_2^{dip}: in $Tb(OH)_3$, C_2 was found to be about $0.1\ C_2^{dip}$. The graph of C_2^{dip}/T^2 is shown in Fig. 7 as C_M/R.

d. Schottky specific heat. The Schottky specific heat, due to the populating of excited states with increasing temperature, can be calculated exactly from the partition function if the energy levels are

known. In his spectroscopic investigation of $Dy(OH)_3$ at 77 K, Scott[4] found that the low-lying excited states occur at energies of 7.8, 21.5, 27.0, and 54.7 cm^{-1}. At 4 K Scott was able to identify only the position of the first excited state, which had shifted to 15.6 cm^{-1}. We have found that our specific-heat data can be accurately accounted for by assuming that only this first excited state has shifted and the positions of the other states remain at 21.5, 27.0, and 54.7 cm^{-1}.

Figure 7 shows a plot of the Schottky specific heat corresponding to the level scheme described above. Also shown in the plot are $(C - C_L)/R$, the experimental result less the lattice estimate. Above 10 K the contribution from C_M is small enough to allow a comparison of the theoretical Schottky estimate with $C - C_L$. The close agreement of C_S with $C - C_L$ is an indication of the accuracy of the assumed energy level scheme.

Further verification for the above energy level scheme is provided by a check of the magnetic entropy, S_M, which is given by

$$\frac{S_M(T)}{R} = \int_0^T \frac{C_M}{RT'}\, dT' , \tag{11}$$

where C_M is the magnetic specific heat. S_M was calculated by numerical integration of the above equation using

$$C_M = C - C_L - C_S - C_{hf} , \tag{12}$$

where C is the total experimental specific heat, and the values of C_L, C_S, and C_{hf} are those given above. The graph of $S_M(T)$ is shown in Fig. 8. Insofar as the assumed values of C_L, C_S, and C_{hf} are accurate, S_M/R at high temperatures should approach the value $0.693 = \ln 2$, the high-temperature limit of a spin-$\frac{1}{2}$ system. In fact, S_M/R very closely approaches this value. The agreement here is particularly impressive in view of the large difference between S_M and the total entropy S_T, which is obtained using C instead of C_M in Eq. (11) and which is also shown in Fig. 8. As this large difference is primarily due to the Schottky specific heat, we have further assurance that the assumed energy level scheme is quite accurate.

C. Discussion

1. Spin Hamiltonian

In treating magnetic systems which have an isolated ground doublet, it is convenient to utilize the formalism of the effective spin-$\frac{1}{2}$ Hamiltonian.[15] For $Dy(OH)_3$ the most general form of the spin Hamiltonian is

$$\mathcal{H}_S = -\sum_i g_{eff}\, \mu_B \vec{H} \cdot \vec{S}'_i - \sum_{\substack{i,j \\ \alpha,\beta}} K_{ij} S'_{i\alpha} S'_{j\beta} , \tag{13}$$

where K_{ij} are the interaction constants, S' is the effective spin-$\frac{1}{2}$, μ_B is the Bohr magneton, and g_{eff} is the effective g value. The sums i and j are over all spins; α and β are sums over the spatial coordinates x, y, and z. The value for g_{eff} may be calculated from

$$g_{eff} = \tfrac{1}{2} g_J \langle s_g \,|\, J_\alpha \,|\, s_g \rangle , \tag{14}$$

where $g_J (= \frac{4}{3})$ is the Dy^{3+} Landé factor and α is x, y, or z. Using the 4.2 K wave function of Table II to calculate the matrix element of J_z in the ground state, we find that the effective g value parallel to the c axis is $g_\parallel = 19.1$. This agrees with the value calculated from the saturation magnetization:

$$g_\parallel = 2M_{sat}/N\mu_B , \tag{15}$$

which gives $g_\parallel = 19.0 \pm 0.2$. The matrix elements of J_x and J_y in the ground states are identically zero, so that $g_\perp = 0.0$.

It is to be expected from the very small hydroxide lattice constants that the predominant interactions in $Dy(OH)_3$ will be the dipole-dipole and the bilinear exchange. Both of these interactions are bilinear in the full Hamiltonian, and within the ground doublet only the J_z terms have nonzero matrix elements. This reduces the spin Hamiltonian to

$$\mathcal{H}_S = -\sum_i g_{eff} H_{zi} S'_{zi} - \sum_{i,j} K_{ij} S'_{zi} S'_{zj} . \tag{16}$$

This simple form is the familiar Ising Hamiltonian. It must be stressed that since the matrix elements of J_x^6 are not completely negligible within the

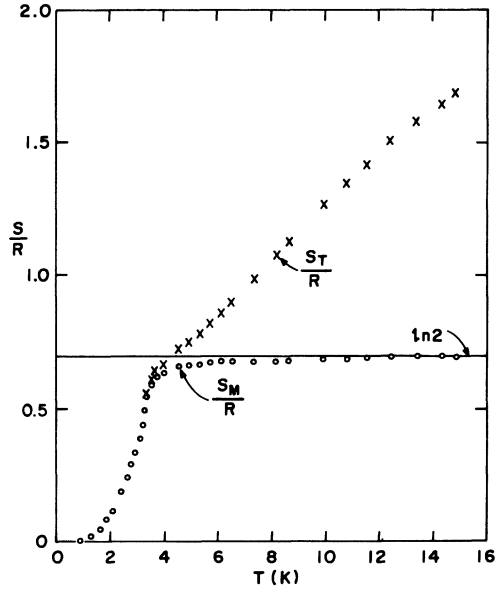

FIG. 8. Experimental curve of entropy in $Dy(OH)_3$. S_M is the magnetic entropy and S_T is the total entropy. S_M/R at high temperatures closely approaches ln2, shown by the solid line in the figure.

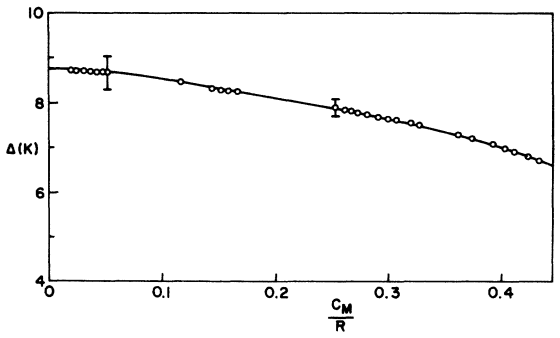

FIG. 9. Ground state splitting Δ of $Dy(OH)_3$ determined from the analysis of the low-temperature specific heat using Eq. (17).

ground doublet, there will be further non-Ising terms in the spin Hamiltonian; but these matrix elements are small and they are related to interactions which are themselves generally second order; for example, biquadratic exchange, virtual-phonon coupling, and anisotropic exchange.

2. *Interaction Constants*

It is sometimes possible to determine the various interaction constants, K_{ij}, from the bulk properties at high temperatures: both the high-temperature magnetic specific heat and the susceptibility are well defined functions of the K's (Ref. 14) and, e.g., in $Tb(OH)_3$ and $Gd(OH)_3$ the K's have been so determined. But in $Dy(OH)_3$ the presence of the low-lying excited states renders such an analysis unfeasible.

One measure of the strength of the interactions, the Curie–Weiss constant Θ, can be obtained from the specific heat at low temperatures, where Schottky effects are negligible. In the limit of zero temperature the specific heat of an Ising system varies as[16]

$$C/R = (\Delta/T)^2 e^{-\Delta/T}, \tag{17}$$

and at $T = 0$, $\Delta = 2\Theta$.

$Dy(OH)_3$ is, as shown above, approximately Ising-like below 4 K. When the low temperature specific heat less the hyperfine contribution was fitted to the above equation,[6] the variation of Δ with C_M near $T = 0$ was found to be as shown in Fig. 9. The curve changes slope steadily but as C_M approaches 0 at low temperatures we can easily read an accurate value for $\Delta(T = 0)$ of 8.8 ± 0.4 K. This leads immediately to

$$\Theta = 4.4 \pm 0.2 \text{ K}.$$

A check on this result for Θ is available from the fact that, for an Ising doublet, the change in magnetic internal energy (in units of R) between $T = 0$ and $T = \infty$ is equivalent to $\frac{1}{2}\Theta$.[17] This energy change can be calculated by an integration of the specific heat

$$U_M(T) = \int_0^T C_M(T')\,dT'. \tag{18}$$

The plot of U_M, obtained by numerical integration of C_M, is shown in Fig. 10. The curve shows a good deal of "meandering" above 6–8 K. This presumably results from the rough estimates of C_L and C_S, and is more severe for the U_M integral than for the faster converging entropy integral [Eq. (11)]. Keeping in mind the fact that the U_M integral should be very accurate up to 6 K where the magnetic effects still dominate C/R, we have estimated the value of $U_M(\infty) - U_M(0)$ to be 2.2 ± 0.2 K, giving a value for the Weiss constant of 4.4 ± 0.4 K. The calculation can be regarded as giving agreement, however roughly, with the value $\Theta = 4.4 \pm 0.2$ K obtained from the low-temperature specific heat. Still a third estimate of Θ is available from Scott,[4] who calculated the $T = 0$ value of Δ from shifts in the spectroscopic transition energy to excited manifolds. Scott's value of $\Theta = 4.9 \pm 0.4$ K is in agreement with the low-temperature specific heat results.

The theoretical expression for Θ, given the Hamiltonian of Eq. (16), is

$$\Theta = \sum_i \tfrac{1}{2} K_i + \sum_i \tfrac{1}{4} g^2 \mu_B^2 \left[(3z^2 - r^2)/r^5\right]_i, \tag{19}$$

where K_i is the nondipolar interaction constant of ith neighbors and the sum i is over all neighbors. Using the known lattice constants and g values, the dipolar contribution—the second term—in Θ was found to be

$$\Theta^{\text{dip}} = 6.14 \text{ K},$$

the positive sign indicating that the net interaction

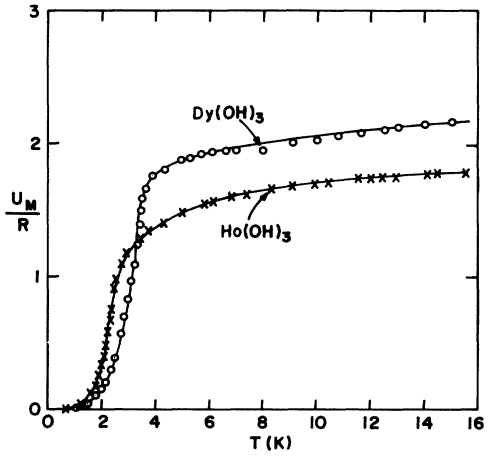

FIG. 10. Change in internal energy as a function of temperature for $Dy(OH)_3$ and $Ho(OH)_3$.

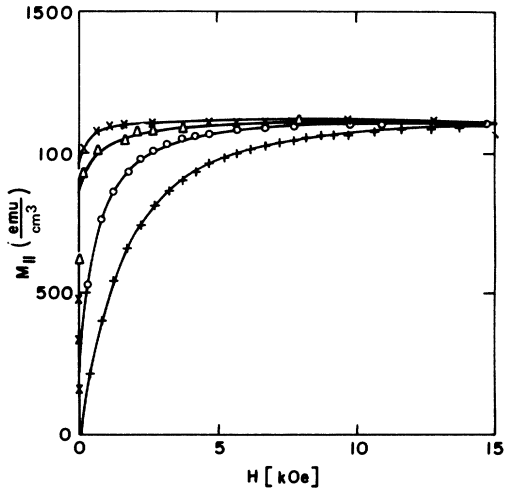

FIG. 11. c-axis magnetization of $Ho(OH)_3$ at high magnetic fields and for a range of temperatures: 4.2 K (+), 3.0 K (○), 2.3 K (△) and 1.1 K (×).

is ferromagnetic. This value, together with the experimental result for Θ, leads to an expression for the sum of the nondipolar interaction constants:

$$\sum_i \tfrac{1}{2}K_i = -1.8 \pm 0.2 \text{ K}.$$

The negative sign of this quantity indicates a net antiferromagnetic contribution to Θ.

In view of the fact that the ordering is ferromagnetic in $Dy(OH)_3$ and the net nondipolar interaction is antiferromagnetic, we are led to conclude that the dipolar interactions play a strong if not dominant role in the ordering phenomena. However, with only a net value for the nondipolar interactions it is not possible to further specify the importance of the individual neighbor interactions in this ordering. Also, in view of the complicating effects of the excited states on the bulk properties, further data on the individual interactions in $Dy(OH)_3$ must await further resonance or spectroscopic studies.

IV. $Ho(OH)_3$: DATA AND ANALYSIS

The C_{3h} crystal field group of the hydroxide lattice imposes the same symmetry restraints on the ground term of Ho^{3+} as on Dy^{3+}: there is admixing only between states differing by 6 in J_z, where z is again along the c axis. Ho^{3+}, however, is a non-Kramers ion (ground term: $4f^{10}$, $^5I_8$) and has allowed singlet states in the hydroxide crystal field; thus the system could *a priori* be diamagnetic at low temperatures, with only a ground state singlet occupied.

In spectroscopic measurements on $Ho(OH)_3$, Scott[4] observed no fluorescence, and all but a few of the absorption transitions appeared as very wide bands. In the absorption spectrum of Ho^{3+} in $Y(OH)_3$ there were sharp transitions from the ground $^5I_8$ manifold to levels of the $^5F_5$, $^5F_4$, and $^5F_3$ manifolds, providing sufficient data for a complete crystal field analysis. The ground state was found to be a true doublet, composed primarily of $|J_z = \pm 7\rangle$ states. There were also found two low-lying excited singlets at energies of 11.1 and 75 cm^{-1}. The lattice constants for $Ho(OH)_3$ and $Y(OH)_3$ are nearly identical, and the crystal field levels identified in $Y(OH)_3$: Ho are expected to be very close to the levels in concentrated $Ho(OH)_3$. Scott's spectroscopic results are summarized in Table II.

Scott also attempted EPR measurements on Ho^{3+} in $Y(OH)_3$ but the linewidths were too large to allow extraction of any useful information.

A. Experimental Results

1. Magnetic Measurements

The high-field magnetization of $Ho(OH)_3$ parallel to the c axis at liquid-helium temperatures is shown in Fig. 11. The sample was a needle-shaped crystal with an aspect ratio of about 16.

The general behavior of the $M_{\parallel}$ curves resembles that in $Dy(OH)_3$: At 4.2 K the curve is not appreciably saturated until ~ 10 kOe; with lower temperature the saturation occurs at lower fields until at 1.1 K there is near-complete saturation at 500 Oe. At this lowest temperature the saturation magnetization of $Ho(OH)_3$ can be accurately read off as

$$M_{sat} = 1140 \pm 20 \text{ emu/cm}^3.$$

There is very little high field slope at 1.1 K, the upper limit on the slope being

$$\chi_{\parallel} < 2 \times 10^{-3} \text{ emu/cm}^3.$$

The magnetic moment with the field perpendicular to the c axis (Fig. 12) is linear over the field range,

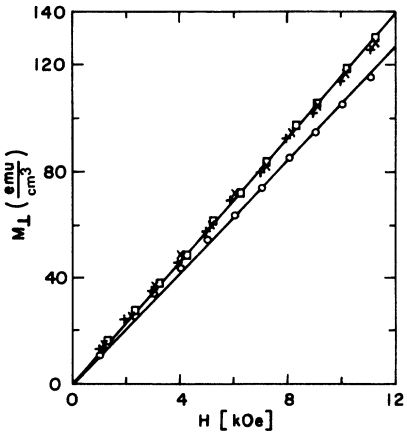

FIG. 12. High-field magnetization of $Ho(OH)_3$ perpendicular to the c axis for the temperatures: 4.2 K (+), 3.0 K (×), 2.3 K (□) and 1.1 K (○).

TABLE III. Susceptibility of $Ho(OH)_3$.

T(K)	χ(Expt.) (emu/cm^3)	Δ (cm^{-1})	χ(Theor.) (emu/cm^3)
4.2	0.0115 ± .003	1.6	0.0132
3.0	0.0115	1.8	0.0134
2.3	0.0115	3.0	0.0127
1.1	0.0104	3.6	0.0120

and at 10 kOe is an order of magnitude less than $M_{\parallel}$ (see Fig. 11). There is also a slight temperature dependence in the slope of $M_{\perp}$, the susceptibility for the temperatures taken being given in Table III.

The large difference between $M_{\parallel}$ and $M_{\perp}$ marks $Ho(OH)_3$ as another very anisotropic system, the magnetic moments being almost totally constrained to lie along the c axis.

The low-field ballistic-galvanometer measurements of M vs H in $Ho(OH)_3$ at 1–4 K provided data for a Kouvel-Fisher analysis, similar to that described for $Dy(OH)_3$ in Sec. III. The zero-field susceptibility parallel to the c axis obtained from this analysis is plotted in Fig. 13 as χ^{-1} vs T. The susceptibility behavior is qualitatively similar to that found for $Dy(OH)_3$: χ^{-1} decreases with decreasing temperature until it assumes a roughly constant value below 2.5 K. We conclude that $Ho(OH)_3$ near this temperature has a transition to an ordered state with the spins aligned along the c axis, and the ordering is probably ferromagnetic. There is no sharp break near 2.5 K but a T^* analysis, as described earlier (Sec. III A), yielded a Curie temperature of

$$T_C = 2.54 \pm 0.01 \text{ K}.$$

The kink in the M^2 vs H_0/M (Sec. III A) curves yielded the plot of spontaneous magnetization as shown in Fig. 4. The low-temperature asymptote of this curve is ~800 emu/cm^3. We thus have much the same discrepancy between M_{sp} and M_{sat} in $Ho(OH)_3$ as in $Dy(OH)_3$, in fact the discrepancy in both cases is 30%. The relation between these effects and irregular sample shape is presumably the same in $Ho(OH)_3$ as in $Dy(OH)_3$ and is discussed in Sec. III.

The low field susceptibility, using the McKim–Wolf inductance technique, was also measured in the liquid-hydrogen-temperature range (14–20 K) and the results are plotted in Fig. 14. As in $Dy(OH)_3$, the effect of the excited states is to introduce a deviation from the Curie–Weiss-law behavior. Once again, lack of precise energy levels and wave function prevents an analysis of χ at these temperatures.

2. *Specific Heat*

The specific heat of $Ho(OH)_3$ between 0.6 and 16 K was measured by the heat-pulse technique and the behavior of C/R vs T is shown in Fig. 15. The prominent spike is due to the magnetic phase transition and is sufficiently well defined to permit accurate determination of the ordering temperature as $T_C = 2.54 \pm 0.01$ K. This value agrees precisely with the susceptibility result, $T_C = 2.54$ K, given earlier.

Above T_C the specific heat is remarkably constant up to about 14 K, at which point it begins to increase slowly. Below T_C, the specific heat de-

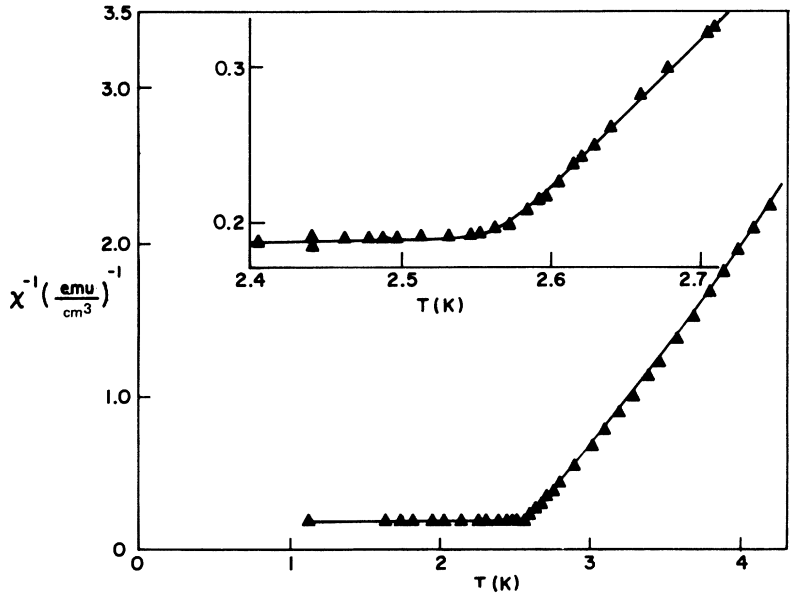

FIG. 13. Susceptibility of $Ho(OH)_3$ in the neighborhood of $T_C = 2.54$ K. The enlarged insert shows no sharp change in behavior at T_C.

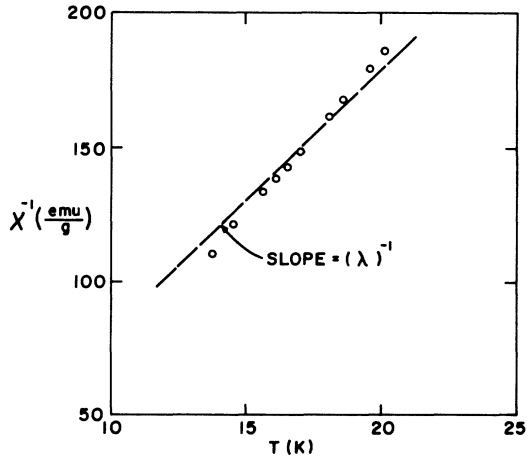

FIG. 14. Susceptibility of $Ho(OH)_3$ along the c axis in the liquid-hydrogen temperature range. The dashed line has the slope of $1/\lambda = 9.6$, the inverse low-temperature Curie constant.

creases down to about 1 K and then increases sharply, indicating a large hyperfine contribution. The individual contributions to C/R will be considered in Sec. IV B.

B. Analysis

1. Magnetic Measurements

Below 4.2 K there is a very slight population of the excited states of $Ho(OH)_3$, the spins being over 99% in the ground doublet; at these temperatures the effective spin-$\frac{1}{2}$ formalism is a good approximation. The wave function for the ground doublet of $Y(OH)_3$: Ho found by Scott[4] is

$$|s_g\rangle = 0.94\,|\pm 7\rangle + 0.31\,|\pm 1\rangle + 0.15\,|\mp 5\rangle.$$

The accuracy of this wave function as an approximation to the ground state of $Ho(OH)_3$ can be estimated by comparing the experimental value of the saturation magnetization, $M_{sat} = 1140 \pm 20$, with M_{sat} found using the above ground state in Eq. (4):

$$M_{sat} = 1125 \text{ emu/cm}^3 .$$

The excellent agreement of this value with the experimental result ($M_{sat} = 1140 \pm 20$) is not surprising in view of the fact that the lattice parameters in $Ho(OH)_3$ are, within experimental error, identical to those in $Y(OH)_3$.[5]

As seen in Figs. 11 and 12, the magnetic moment perpendicular to the c axis is an order of magnitude smaller than the parallel moment. In fact, the matrix element of J_x within the ground doublet is identically zero, so that even the small observed $M_\perp$ cannot be due to the direct moment. It must instead be due to the Van Vleck susceptibility which arises out of the mixing of the excited-state wave functions into the ground state via the Zeeman Hamiltonian. The general expression for this Van Vleck term is

$$\chi_{VV}^{\alpha} = 2Ng_J^2\mu_B^2 \left[\sum_\gamma \sum_\nu |\langle \gamma | J_\alpha | \nu \rangle|^2 \times e^{-E_\gamma/kT}/(E_\nu - E_\gamma) \right] \Big/ \sum_\gamma e^{-E_\gamma/kT} , \quad (20)$$

where α is a spatial direction; $\sum_\gamma$, $\sum_\nu$ are sums over all the states; g_J is the Landé factor, and μ_B the Bohr magneton. For cases in which the ground doublet is isolated and degenerate, χ_{VV} reduces to the familiar temperature-independent form. Scott[4] has shown that below 2.5 K in $Ho(OH)_3$ the ground doublet becomes increasingly more split, due to the phase transition which will be described below; Scott's values for the splitting, Δ, are given in Table III, along with the value of χ_{VV} calculated from Eq. (20).

The wave functions and energy levels used in this calculation are those given in Table II for $Y(OH)_3$: Ho. The agreement between the experimental and theoretical values is reasonably good, although there is a small discrepancy of about 15%, undoubtedly due to the lack of complete correspondence between the crystal fields in $Ho(OH)_3$ and $Y(OH)_3$: Ho. But the relative change in χ_{VV} with temperature (~ 10%), which depends primarily on the ground state splitting, is accurately predicted by the theory.

2. Specific Heat

The total specific heat consists of four contributions, each of which is considered individually.

a. Hyperfine. The specific heat below 1 K is seen to be rising sharply with decreasing temperature, indicating that the hyperfine specific heat is contributing strongly. In order to accurately ac-

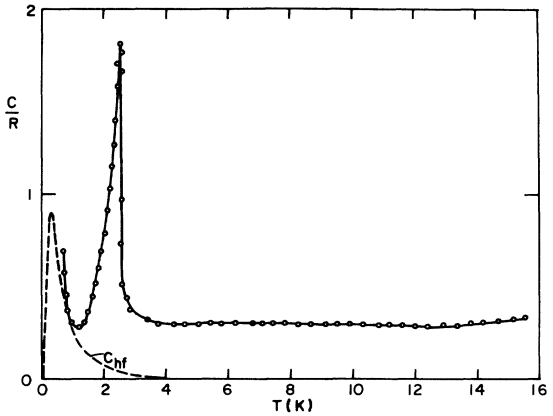

FIG. 15. Specific heat of $Ho(OH)_3$. The prominent spike defines the Curie temperature at 2.54 K. The dashed curve is the theoretical Ising hyperfine specific heat [Eq. (21)].

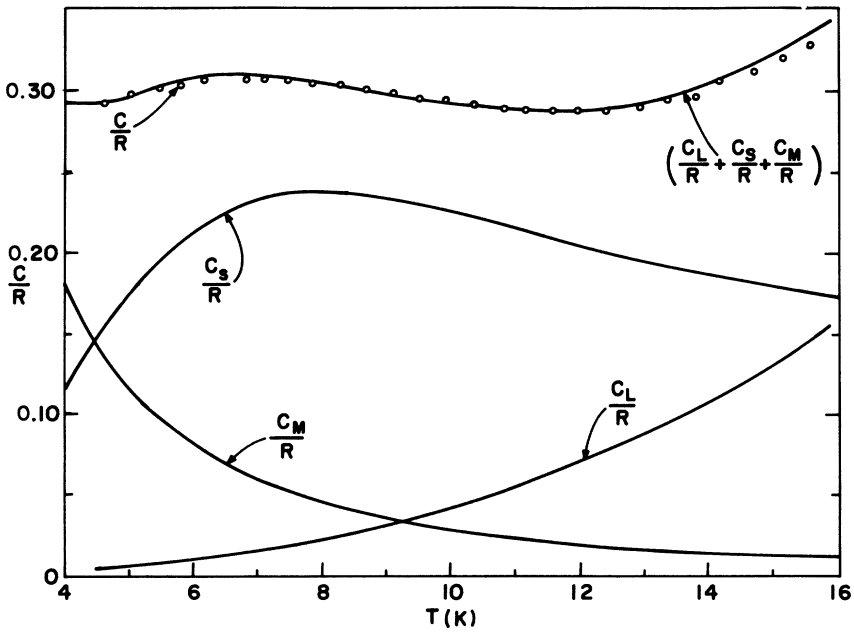

FIG. 16. Estimates of the lattice (C_L), Schottky (C_S), and magnetic (C_M) contributions to the specific heat above T_C. Also shown is the sum of these three ($C_M + C_L + C_S$) which agrees accurately with the experimental points, shown as dots.

count for this contribution we have taken advantage of the Ising character of $Ho(OH)_3$ (see Sec. IV C) and used the expression for the hyperfine specific heat of an Ising system as given by Mattis and Wolf[18]:

$$C_{hf} = -\frac{AI}{2}\frac{d}{dT}B_I\left(\frac{AI}{kT}\right), \tag{21}$$

where A is the interaction constant of Eq. (6) and B_I is the Ith-order Brillouin function. The value of A for $Ho(OH)_3$ was calculated from Eq. (8) using the value of A/g from Table I. The behavior of the calculated $C_{hf}(T)$ is shown in Fig. 15. At the lowest temperatures, C_{hf} fails to account for all of the hyperfine bump, indicating that our estimate of C_{hf} is not entirely accurate. The remainder cannot be accounted for by adjusting A. It is probably due to the fact that $Ho(OH)_3$ is Ising-like only to a first approximation, and that non-Ising terms in the Hamiltonian limit Eq. (21) to being a first approximation to C_{hf} in $Ho(OH)_3$.

b. Lattice. The lattice specific heat will be approximated by the total specific heat of $La(OH)_3$, as explained in Sec. III.

c. Magnetic and Schottky specific heats. A large Schottky specific heat C_S in $Ho(OH)_3$ was expected because of the low-lying energy levels. There is also a magnetic contribution C_M which at high temperatures will vary as $1/T^2$. Using the levels for Ho^{3+} in $Y(OH)_3$ as a starting point, an iteration was done varying the $1/T^2$ magnetic specific heat coefficient and the lowest excited energy level until a good fit to the experimental data was obtained. This fit is shown in Fig. 16 along with the individual magnetic, Schottky, and lattice contributions. C_M here has the functional behavior $2.9/T^2$, C_S corresponds to levels at 17.0 K and 105 K, and the lattice contribution is exactly that of $La(OH)_3$. While this fit is by no means unique, the fact that the three contributions have such different temperature dependences means that it is not possible to compensate for a large change in one with changes in the other two. There is thus some assurance that the exact solution is not very different from that assumed above.

An independent check on the validity of this solution is provided by a calculation of the magnetic entropy by numerical integration of Eq. (11), again using Eq. (12) for C_M. $S_M(T)$ is shown in Fig. 17. At 15 K, $S_M = 0.679$. To extrapolate to $S_M(\infty)$ we have added the high-temperature effect of the $1/T^2$ term in Eq. (11) and find a value $S_M(\infty) = 0.683$. This value is reassuringly close to the value $\ln 2 = 0.693$ expected for the exact solution of an isolated ground doublet.

Below 3 K the specific heat is overwhelmingly magnetic in origin and the calculations of magnetic entropy should be very accurate in this range. At T_C the magnetic entropy has a value of only 0.48, implying a good deal of short-range order in the system above T_C. This is in comparison to $Dy(OH)_3$ and $Tb(OH)_3$, both of which showed entropy values of 0.58 at T_C. This high degree of short-range order was verified by Scott, who estimated[4] the ground-state splittings in $Ho(OH)_3$ from shifts in the absorption spectrum of the $^5I_4$ manifold: At 4.2 K the ground-doublet splitting was already 1.6 cm^{-1}, and it increased to 3.0 cm^{-1} at T_C (Table III).

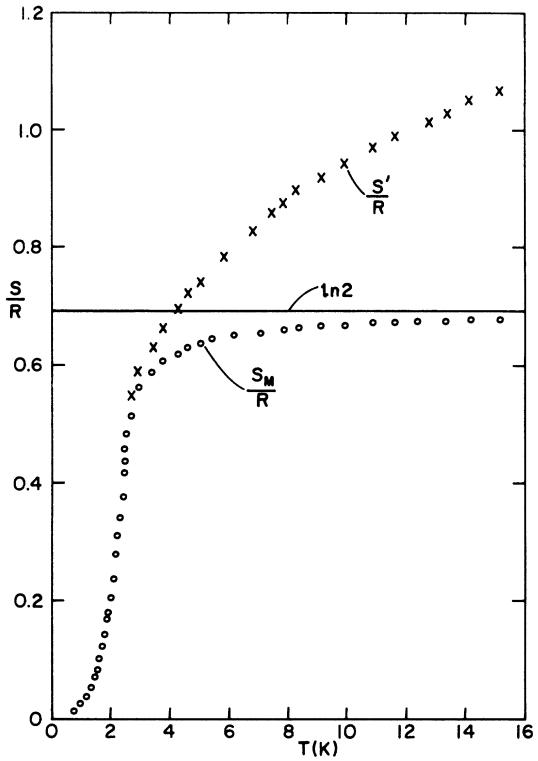

FIG. 17. Experimental values for the entropy of $Ho(OH)_3$. S_M is the magnetic entropy and S' is the total entropy minus the hyperfine entropy. S_M/R at high temperatures closely approaches ln2, shown by the solid line in the figure.

C. Discussion

1. Spin Hamiltonian

At 4 K, $Ho(OH)_3$ has virtually all of the spins occupying the ground doublet. It thus becomes possible to employ the effective spin-$\frac{1}{2}$ formalism and use the Hamiltonian of Eq. (13). The effective g value, which is calculated from Eq. (14) using the eigenfunction of Table II and $g_J = \frac{5}{4}$, is

$$g_{\parallel} = 15.3 .$$

This is in good agreement with the experimental value

$$g_{\parallel} = 15.5 \pm 0.2$$

calculated using Eq. (15) and the experimental value of M_{sat}.

While the ground-state eigenfunction is primarily $J_z = \pm 7$, there is considerable admixing of both the $|\pm 1\rangle$ and $|\mp 5\rangle$ states. Within this ground doublet the matrix elements of operators of J_x^2 and J_x^6 are of a magnitude comparable to those of J_z. However, the small size of the hydroxide lattice suggests that the predominant interactions are probably the bilinear exchange and dipolar couplings. So it is expected that to first order the effective spin Hamiltonian of $Ho(OH)_3$ may be approximated by Eq. (15), the Ising Hamiltonian. It should be stressed that, in view of the large admixing within the ground doublet, the Ising Hamiltonian is only a first approximation, and a rather weak one compared to $Tb(OH)_3$ and even $Dy(OH)_3$; however, for the sake of some calculations, it is a useful one.

2. Interaction Constants

In $Ho(OH)_3$, as in $Dy(OH)_3$, the presence of the low-lying excited states precludes an accurate determination of the interaction constants from the analysis of bulk properties at high temperatures. In $Ho(OH)_3$ there is the additional complication of a large hyperfine specific heat eliminating the possibility of determining Θ from a fit of Eq. (16) at low temperatures.

A rough estimate of Θ is available from the calculation of $U_M(\infty) - U_M(0)$, as described in Sec. III. The variation of $U_M(T)$, calculated by numerical integration of Eq. (18), is shown in Fig. 10. The value of $U_M(\infty)$ may be estimated more closely by adding to U_M at 10 K, the contribution from the first-order specific-heat term. Using the estimate of $C_2 = 2.9$ from Sec. IV B we get $U_M(\infty)/R = 2.0$ and

$$\Theta = 4.0 \pm 0.4 \text{ K} .$$

The dipolar contribution to Θ, calculated from Eq. (19), is 4.4 K, which leaves a value of -0.4 K for the nondipolar contribution.

We thus have much the same situation in $Ho(OH)_3$, with regard to the interaction constants, as we had in $Dy(OH)_3$. The experimental value for Θ is ferromagnetic in sign and smaller than the net dipolar Θ; this leads to a net nondipolar contribution which is negative, favoring antiferromagnetic ordering. Since the actual ordering is ferromagnetic we conclude that the dipolar interaction plays a very large, if not dominant, role in the ordering of $Ho(OH)_3$.

V. SUMMARY AND CONCLUSION

The result of the present study has been the characterization of the magnetic effects in $Dy(OH)_3$ and $Ho(OH)_3$ through the measurement and analysis of the magnetic susceptibility and specific heat at low temperatures. The important numerical results are summarized in Table IV.

$Dy(OH)_3$ has been shown to be highly anisotropic below 4 K, with virtually zero component of magnetization perpendicular to the c axis. At 3.48 K this compound undergoes a phase transition to a ferromagnetic ordered state. The effective spin Hamiltonian is, to a first approximation, Ising-like in form; from a comparison of the experimental Weiss Θ ($= +4.4$ K) with the theoretical dipolar Θ ($= 6.14$ K) it was shown that the dominant

TABLE IV. Summary of experimental results.

	$Dy(OH)_3$	$Ho(OH)_3$
M_{sat}	1405 ± 15 emu/cm^3	1140 ± 20 emu/cm^3
$g_{\parallel}$	19.0 ± 0.2	15.5 ± 0.2
$g_{\perp}$	0.0	0.0
$\chi_{\perp}(T=1.1\ K)$	5×10^{-4} emu/cm^3	1.0×10^{-2} emu/cm^3
T_C	3.48 ± 0.01 K	2.54 ± 0.01 K
$A_{(hyperfine)}$	0.075 (Dy^{161})	0.47 (Ho^{165})
	0.104 (Dy^{163})	
Θ		
($\Delta/2$ from specific heat)	4.4 ± 0.2 K	•••
($\Delta/2$ from spectroscopy)	4.9 ± 0.6 K	•••
(from U_M/R)	4.4 ± 0.4 K	4.0 ± 0.4 K
Θ (dipolar only)	6.14 K	4.4 K
Θ (nondipolar)	−1.8 ± 0.2 K	−0.2 ± 0.4 K

interaction in the Hamiltonian is the dipolar interaction. At temperatures above 4 K the bulk properties are strongly influenced by the presence of low-lying excited states. Using a spectroscopic energy level scheme of Scott[4] it was shown possible to accurately account not only for the effects of the excited states on the specific heat, but also for much of the detailed behavior due to the ground doublet.

$Ho(OH)_3$ was found to be, in many respects, very similar to $Dy(OH)_3$. In particular the high anisotropy, the ferromagnetic ordering ($T_C = 2.54$ K), the dominant dipolar interactions ($\Theta = 4.0$ K, $\Theta^{dip} = 4.4$ K), and the strong influence of low-lying excited states are all characteristic of $Ho(OH)_3$ as well. And once again using the spectroscopic results reported by Scott,[4] good agreement between the observed bulk properties and the underlying energy level scheme was observed.

ACKNOWLEDGMENTS

We would like to thank S. Mroczkowski and J. Eckert for growing the crystals used in these experiments, and C. Schneider for his skillful help in the construction and maintenance of the apparatus. We are also indebted to Dr. P. D. Scott for allowing us to quote his unpublished spectroscopic data. And finally, we owe a special thanks to Professor W. P. Wolf for his support, help, and encouragement throughout the course of this work.

---

†Based on Ph.D. theses submitted by C. A. Catanese and H. E. Meissner to the Yale University Graduate School. Work supported in part by the U.S. Atomic Energy Commission and in part by the National Science Foundation.

*Present address: RCA Laboratories, Princeton, N. J. 08540.

‡Present address: Corning Glass Works, Corning, N. Y. 14830.

[1]W. P. Wolf, H. Meissner, and C. A. Catanese, J. Appl. Phys. **39**, 1134 (1968).

[2]C. A. Catanese, A. J. Skjeltorp, H. E. Meissner, and W. P. Wolf, Phys. Rev. B (to be published).

[3]A. J. Skjeltorp, C. A. Catanese, H. E. Meissner, and W. P. Wolf, Phys. Rev. B **7**, 2062 (1973).

[4]P. D. Scott, dissertation (Yale University, 1970) (unpublished).

[5]P. V. Klevtsov and L. P. Sheina, Neorg. Materialy **1**, 912 (1965).

[6]D. P. Landau, B. E. Keen, B. Schneider, and W. P. Wolf, Phys. Rev. B **3**, 2310 (1971).

[7]F. R. McKim and W. P. Wolf, J. Sci. Instrum. **34**, 64 (1957).

[8]K. P. Belov and A. N. Goryaga, Fiz. Met. Metalloved. **2**, 3 (1956).

[9]J. S. Kouvel and M. E. Fisher, Phys. Rev. **136**, A1626 (1964).

[10]B. Bleaney, Phys. Rev. **78**, 214 (1950).

[11]R. J. Elliott and K. W. H. Stevens, Proc. R. Soc. A **218**, 553 (1953).

[12]A. H. Cooke, D. J. Edmonds, F. R. McKim, and W. P. Wolf, Proc. R. Soc. A **252**, 246 (1959).

[13]The compounds used in this investigation of lattice specific heat were: La, Nd, Gd, Tb, and Er hydroxide. At any given temperature in the range 4–15 K, the lattice specific heats were found to vary by less than 15% over the whole group of compounds.

[14]J. M. Daniels, Proc. R. Soc. A **66**, 673 (1953).

[15]K. W. H. Stevens, *Magnetism I*, edited by G. T. Rado and H. Suhl (Academic, New York, 1963), p. 1.

[16]A. J. Wakefield, Proc. Camb. Philos. Soc. **47**, 419 (1951).

[17]G. Garton, M. J. M. Leask, W. P. Wolf, and A. F. G. Wyatt, J. Appl. Phys. **34**, 1083 (1963).

[18]D. Mattis and W. P. Wolf, Phys. Rev. Lett. **16**, 899 (1966).